View metadata, citation and similar papers at core.ac.uk

brought to you by CORE

provided by Elsevier - Publisher Connector

Available online at www.sciencedirect.com

SciVerse ScienceDirect

Energy Procedia 10 (2011) 271 – 281

Energy Procedia

European Materials Research Society Conference
Symp. Advanced Inorganic Materials and Concepts for Photovoltaics

A ultra-thin silicon nitride barrier layer implementation for silicon quantum dots in amorphous silicon carbide matrix in photovoltaic application

Zhenyu Wan[a]*, Shujuan Huang, Martin Green, Gavin Conibeer

a. *School of Photovoltaics and Renewable energy, University of New South Wales, Sydney 2032, NSW, Australia*

Abstract

To search a suitable material candidate for "all-Si" tandem solar cell, a hybrid super-lattice structure consisting 30 periods of alternating amorphous $Si_{0.7}C_{0.3}$ (5nm) layers and ultra-thin Si_3N_4 barrier layers (0.2-2.0nm) has been deposited by magnetron sputtering with subsequent annealing by a rapid thermal annealing (RTA) process. Structural and electrical characterization of the layered film was carried out after annealing. 8nm barrier layer thickness is proven to be able to provide sufficient structural confinement even after high temperature annealing. Increased resistivity was measured for the overall multi-layer structure, resulting from the incorporation of the Si_3N_4 barrier layers hence likely suppressing carrier transport and further electron hopping is proven the main transportation mechanism.

© 2011 Published by Elsevier Ltd. Open access under CC BY-NC-ND license.
Selection and/or peer-review under responsibility of Organizers of European Materials Research Society (EMRS) Conference: Symposium on Advanced Inorganic Materials and Concepts for Photovoltaics.

Key words: Si nanocrystal, SiC matrix, hybrid structure, superlattice structure

1. Introduction

Materials involving silicon quantum dots embedded in a silicon carbide (SiC) matrix have attracted the attention of many researchers especially for photovoltaic applications because of the possibility of a

* Corresponding author. Tel.: +61 293856782; fax: +61 293855104.
E-mail address: z.wan@student.unsw.edu.au.

1876-6102© 2011 Published by Elsevier Ltd. Selection and/or peer-review under responsibility of Organizers of European Materials Research Society (EMRS) Conference: Symposium on Advanced Inorganic Materials and Concepts for Photovoltaics. Open access under CC BY-NC-ND license.
doi:10.1016/j.egypro.2011.10.190

tunable optical band gap [1-4]. SiC has a much lower band gap at 2.5eV compared with other dielectric matrix materials such as Si_3N_4 and SiO_2 (bandgaps of 5.3eV and 9eV respectively). Therefore quantum dots in a SiC matrix are confined by a much lower barrier height and hence tunneling probability between adjacent quantum dots is enhanced (exponentially by the decrease in barrier height). Thus there is potential for more conductive devices to be fabricated using a SiC matrix as compared to Si_3N_4 or SiO_2 matrices.

In the previous research of some of the current authors, a super-lattice structure of amorphous silicon rich carbide (Si_xC_{1-x}) layers and SiC barrier layers has been fabricated by magnetron sputtering [5]. Si nanocrystals (Si-NCs) can then be precipitated from the Si rich layer during a furnace anneal at 1100^{o}C. However, nanocrystalline β-SiC particles are also formed in the SiC barrier layers. In addition, the super lattice structure is compromised by substantial Si inter-diffusion resulting in excessive growth of the Si NCs such that they can bridge across the SiC barrier layers. Si NCs with diameters greater than the layer thickness are observed, suggesting that stoichometric SiC does not perform effectively as a diffusion barrier for Si.

The Kurokawa group [4] has also reported that β-SiC lead to a significant current leakage along the SiC grain boundaries when using PECVD followed by high temperature annealing. Oxygen atoms were successfully introduced using CO_2 gas to suppress the SiC barrier crystallization, but the residual oxygen related donors[6] and high band gap of SiO_2 may also introduce a number of other difficulties. Recently, Cheng's group [3] has reported their fabrication of Si-NC in a-SiC matrix with PECVD at 200^{o}C. SiC NCs can be detected in the film due to the low annealing temperature. However, the average distance between Si NCs is large (more than 8nm) from the reported TEM image while electrical characterization has not been reported.

From the discussion in the last chapter, we observed a very serious SiC crystallization in super-latticed SRC / SiC structure. Possible negative impacts have been discussed regarding to the very flat I-V curve from the aspect of p-n junction interface, local defects, as well as residual strains.

Si_3N_4 is a material with very low diffusion coefficient which has been widely used in semiconductor industry as a barrier layer. As a result, there is an approach to achieving good spatial confinement of the Si-NCs, and also minimizing crystallization of β-SiC grains, is the incorporation of Si_3N_4 barrier layers to inhibit Si diffusion.

In this structure, we are aiming to entirely confine the Si NCs grain size and minimize the SiC crystallization by introducing Si_3N_4 material as a diffusion barrier rather than SiC. And consequently, the problems mentioned above would be expected to be largely controlled.

2. Fabrication / structural characterization of UT-SiN structure sample

In this work, alternate layers of amorphous $Si_{0.7}C_{0.3}$ and ultra-thin Si3N4 (UT-SiN) multi-layer super lattice structures were deposited using a magnetron AJA-2200 sputter system. The detailed multilayer structures with 30 periodic bi-layers (Si_xC_{1-x} / UT-SiN) of all samples are listed in Table 1. Both (100)-oriented Si wafer and quartz plates were used as substrates. Each $Si_{0.7}C_{0.3}$ layer (~5nm) was co-sputtered using Si and SiC targets with a separately tuneable RF power ratio for each, while the Si_3N_4 barrier layer (0.2~2.0nm) was sputtered from a single Si_3N_4 target. The samples were not intentionally heated during

sputtering. Rapid thermal annealing (RTA) has been reported as a good crystallization technique for NC systems and all samples were annealed by RTA at 1100^{o}C for 2 minute in a nitrogen atmosphere.

The structural properties have been investigated by X-ray diffraction (XRD) and transmission electron microscopy (TEM) to determine the degree of Si-NC size confinement after high temperature annealing.

Sample Name	$Si_{0.7}C_{0.3}$ thickness (nm)	UT-SiN layer thickness (nm)
UT-SiN0.2	5.0	0.2
UT-SiN0.5	5.0	0.5
UT-SiN0.8	5.0	0.8
UT-SiN2.0	5.0	2.0

Table 1 Sample name and detailed structure. All samples consist of 30 periodic bi-layers

TEM investigation

Figure 1(a) and (b) shows the HRTEM images of a cross-sectional view of sample UT-SiN0.2 and UT-SiN2.0. Clear fringes from Si-NCs can be observed in both images with a typical spacing of 3.1Å which corresponds to (111) lattice planes of Si. In the UT-SiN0.2 sample, the layered structure apparently was destroyed after annealing as shown by the insert in Figure 1(a). The observed Si-NCs are randomly positioned and the grain size has exceeded the initially deposited $Si_{0.7}C_{0.3}$ layer thickness.

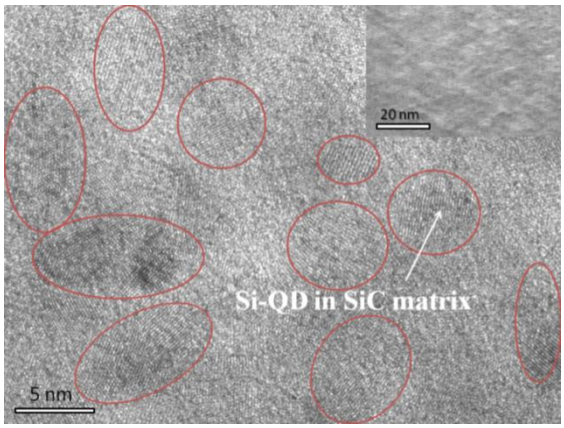

Figure 1 (a) Cross-sectional TEM image of the UT-SiN0.2 sample. The average diameter of the Si-NCs is about 11 nm. The NCs are randomly arranged and no layer interfaces are visible. (Insert: 20nm scale cross-sectional view, the layer edge is blurred)

On the contrary, in the UT-SiN2.0 sample, the clear periodic super-lattice structure is still well preserved after high temperature annealing. Furthermore, all Si-NCs are well constrained in the $Si_{0.7}C_{0.3}$ layers and grain sizes are confined to the 5nm in diameter or smaller of the initially deposited layer. Compared with UT-SiN0.2 sample, UT-SiN2.0 sample shows a much clearer layer edge, indicating that layer inter-diffusion can be suppressed by the 2nm thick Si_3N_4 barrier layer.

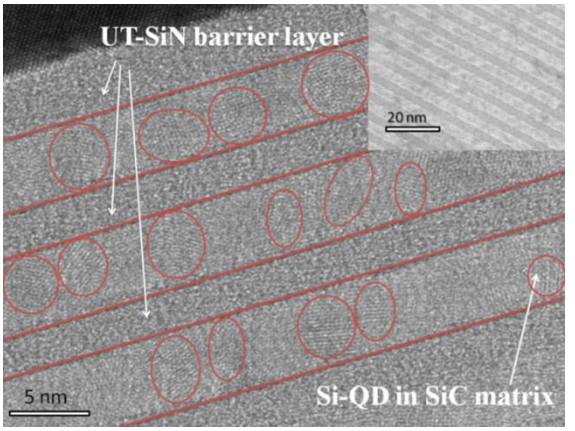

Figure 1 (b) TEM cross-section image of the UT-SiN 2.0nm sample. The super-lattice structure and Si-NC confined to the layers can be clearly observed (Insert: 20nm scale cross-sectional view, the layer edge is clear)

XRD investigation

The NC diameter was estimated quantitatively using fits to XRD peaks and the Scherrer formula. The trend in Figure 2 can be explained in terms of NC nucleation and growth mechanisms. The formation of Si or β-SiC NCs is widely recognized as a two-step process. First, nucleation or cluster formation occurs by very localized atomic rearrangement at short times [3]. Next, NCs grow by diffusion of atoms over longer distances and times to nucleation sites [7-8]. Si has a lower diffusion coefficient in amorphous Si_3N_4 than in SiC [9]. When the Si_3N_4 barrier layer is absent, a-Si and a-SiC can easily inter-diffuse and nucleation points occur uniformly throughout the whole film. As a result, at high temperatures both Si and β-SiC NCs are precipitated with equal probability. Due to the strain in the matrix, SiC NCs cannot grow over 2nm. A similar result calculated (a critical size of NC about 2nm) from the classical theory of nucleation discussed by the Riabinina group [10].

From the grain size calculation, the minimum thickness for a Si_3N_4 barrier layer to prevent Si inter-diffusion is between 0.5nm-0.8nm. Also, the elimination of β-SiC NCs from XRD analysis can be explained. When the Si_3N_4 barrier is over 0.8nm, inter-diffusion is prevented. The high Si concentration in silicon rich layers also suppresses the growth of β-SiC NCs. The XRD shows these to be no larger than 2nm in diameter.

The large amount of lattice mismatch between crystalline Si and SiC means that in the event of both crystallizing into NCs with relaxed lattice parameters, there is not any sharing of strain energy across the whole structure. But a structure in which only one species crystallizes allows the induced strain to be shared across the amorphous matrix and perhaps paradoxically result in a more homogenous and overall evenly strained structure. The excessive Si in the $Si_{0.7}C_{0.3}$ layers forces this crystallization to be of the Si rather than SiC. The role played by the Si_3N_4 barrier layers is to ensure this localized excess of Si remains in the SRC layers and hence ensures the crystallization of Si NCs rather than SiC NCs.

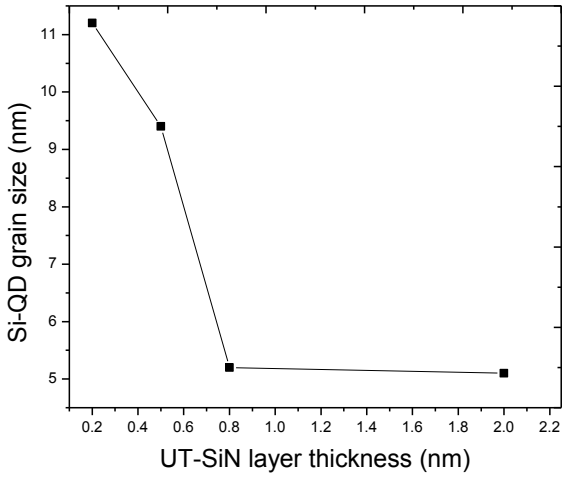

Figure 2 XRD analysis and corresponding crystallite sizes from the Scherrer formula for all the Si3N4 barrier thicknesses. Insert: Si (111) and SiC (111) peaks of each sample. The grain size stops decreasing when the Si_3N_4 thickness is more than 0.8nm

XRR investigation

The XRR characterization has been applied to investigate the quality of layer interface and super-latticed structure of the group of samples with different Si_3N_4 barrier thickness. Figure 3 (a) provides the XRR curve of the sample group before annealing: similar as the SRC / SiC structure, clear super lattice structure is revealed from the clear and periodical distributed Bragg peaks and Kiessing fringes. The slight peak shift in 2 θ position of the Bragg peaks is because of the thickness variation of Si_3N_4 barrier layer.

After annealing, XRR measurement is also applied with same system configuration. As shown in Figure 3 (b), in sample UT-SiN0.2 and UT-SiN0.5, the Bragg peaks can barely been seen at the high order angle region. This phenomenon can be explained as the increasing roughness of layer interface, which leads to the un-uniformed scattering of X-ray reflection, especially in high order angle position where the intensity of X-ray signal is relative low.

Compare with the two samples discussed before, sample UT-SiN0.8 and UT-SiN2.0 still behaves significant Bragg peaks in all range of 2 θ , which indicating that after high temperature annealing process, the super-lattice structure still well preserved from the point of clear XRR peaks can be observed due to the reflective interface between SRC and Si_3N_4 layers.

Thus we may conclude that the critical thickness for the Si_3N_4 barrier is about 0.8nm. Based on the super-lattice structure crystallization mechanism we discussed in previous chapters, the SiC inter-diffusion step can be almost prevented even in high temperature annealing process when the thickness of Si_3N_4 barrier increases over this critical value. As a result, the SiC NC formation could also be prevented due to the insufficient amorphous SiC in each SRC layer.

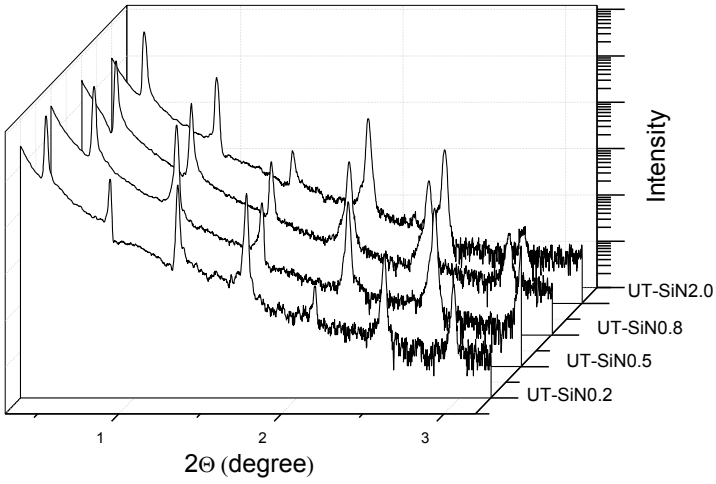

Figure 3 (a) XRR curves of samples with different Si3N4 barrier thickness before annealing

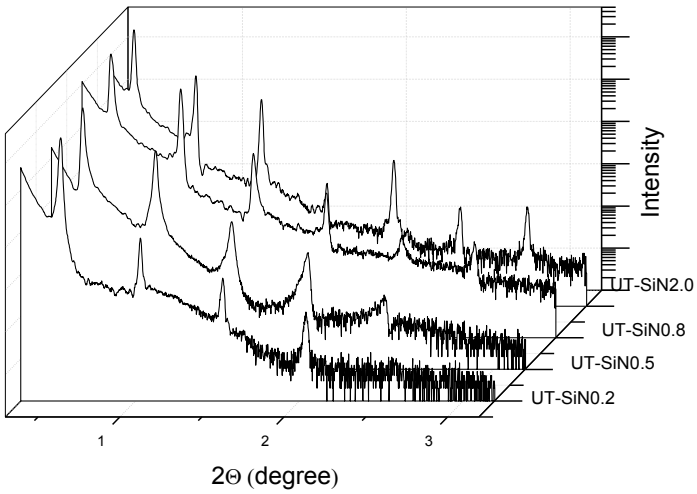

Figure 3 (b) XRR curves of samples with different Si3N4 barrier thickness after annealing

XPS investigation

XPS measurements were carried out to analyze the size-dependent C 1s, Si 2p core-level spectra of Si NCs and SiC NCs in this super-lattice structure. Researchers have reported the relationship between Si 2p core-levels shift by XPS analysis and grain size in Si NCs embedded in dielectric system [11].

In the super lattice system, similar results are observed in both Si element as well as C element. In Figure 4 (a), clear peak shift is behaved on C 1s peak as we can see. Two main peaks can be de-convoluted into [12], including peak I which occurs at 282.7eV ~ 283.2eV can be attributed to C bonded to Si in SiC and peak II which occurs at 284.6eV which is attributed to either C in graphite or hydrocarbons (CH_2) which maybe induced adventitiously. Similar to the conclusion in previous experiments, when Si_3N_4 barrier thickness grow above 0.8nm, C peak II is generally disappeared because of the absence of SiC NCs in the matrix.

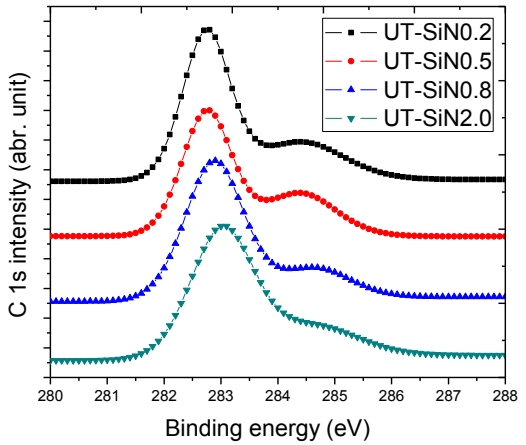

Figure 4 (a) Si peak shift trend with different Si_3N_4 barrier layer thickness in XPS characterization

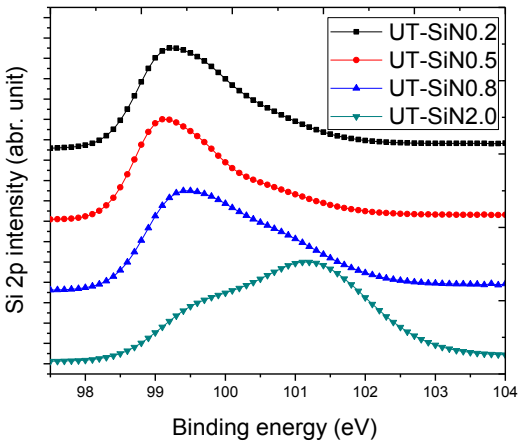

Figure 4 (b) Si peak shift trend with different Si_3N_4 barrier layer thickness in XPS characterization

Similar explanation can be concluded regarding to Si 2p peak analysis. Several main peaks can be de-convoluted from the XPS results including Si^{0+} at 99.78eV, Si^{1+} at 100.55eV and Si^{2+} at 101.50eV [11]. In Figure 4 (b), significant peak shift can be observed when Si3N4 layer thickness increase over 0.8nm where the Si NC grain size can be effectively confined and SiC NCs are eliminated. The peak shift trend is well matched with the references [11, 13-14] which can further confirm the influence from grain size change.

Electrical characterization of multilayer structure

Electrical characterization has been performed to investigate the possible transport mechanism in the multilayer structure. Aluminum contacts with different spacing were evaporated onto films made on quartz substrates. The metal contacts were annealed at 500^{o}C in Ar/H_2 atmosphere for 40mins to ensure ohmic behavior [15].

The top view of the metal contact pattern is illustrated as the insert of Figure 6 (a). The transfer length model (TLM) was used to measure the resistivity. Figure 6 (a) shows that the resistivity increased dramatically (about 2 orders of magnitude) when Si_3N_4 barrier thickness increases from 0.2nm to 2.0nm. The change of resistivity can be explained with respect to various carrier transport mechanisms [4, 16], including tunneling through barriers, tunneling under coulomb blockade and various kinds of hopping space charge transport and leakage. As we know, carrier tunneling is a process temperature independent. As a result, the two dimensional correlated hopping mechanism in our structure has been quantitatively studied. The A.I.Yakimov group[17] pointed out that the Efros-Shklovskii behavior could be used to evaluate the hopping effect.

$$(T) = б_0 \exp [-(T_0/T)^2] + б_1 \qquad (1)$$

Where T is the temperature, T_0 which is proportional to $(K\xi)^{-1}$ is the characteristic interaction energy scale, $б_0$ is film conductivity, K is the relative permittivity of the host lattice, ξ is the localization length of electrons and $б_1$ is the conductivity contributed from other temperature independent factors. We plot the curve of Log б versus $T^{-1/2}$ to extract the T_0 value and compare transport in different samples.

As Figure 6 (b) shows, б (T) is proportional to $T^{-1/2}$ in all samples, indicating that hopping is one of the main transport mechanisms. T_0 increases dramatically as Si_3N_4 barrier thickness increases from 0.2nm to 0.5nm then stabilizes until the Si_3N_4 barrier increases up to 2.0nm. It should be noted here that, both vertical and lateral conductivity are measured in this technique, but as the Si richness and grain size are almost the same in most samples (especially in UT-SiN0.5, UT-SiN0.8, UT-SiN2.0), lateral conductivity is considered to be roughly the same.

Thus vertical conductivity in this system can be compared based on overall conductivity results. Compared with the almost linear growth trend of overall resistivity, we consider this phenomenon could result from the differing increasing vertical inter-dot distance as the Si_3N_4 thickness increases.

As can be seen in the TEM images of Figure 1, when the Si_3N_4 barrier layer is very thin (0.2-0.5nm), the inter-dot distance is very small (less than 0.5nm) or the dots may even be in physical contact. In this

case different tunneling mechanism is likely to be involved and carrier hopping between Si NCs may not be the dominant transport mechanism.

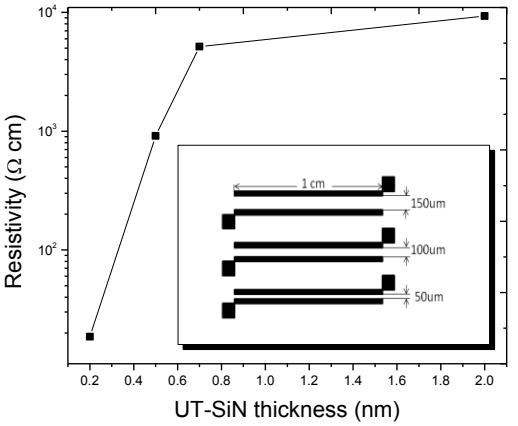

Figure 6 (a) Resistivity of all Si_3N_4 barrier thickness samples in room temperature (insert: top view of Al contact pattern)

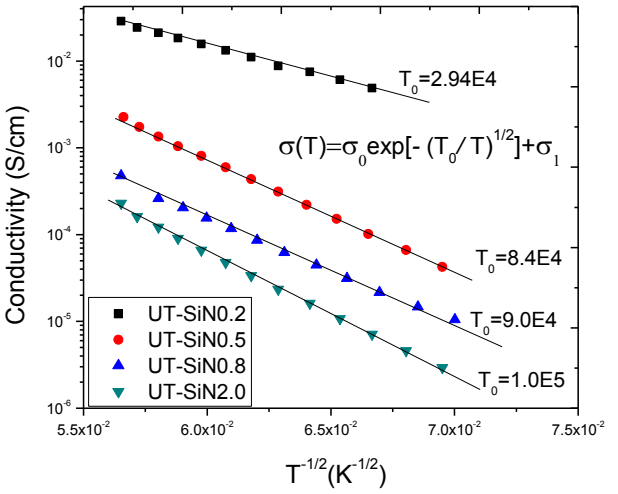

Figure 6 (b) Temperature-IV measurements for different Si3N4 barrier thickness, in the formula: б - film conductivity, $б_0$ – prefactor, $б_1$ – conductivity induced by other factors, T_0 - characteristic interaction energy scale. T_0 increase rapidly when Si_3N_4 barrier increase from 0.2nm to 0.5nm, then stays the same.

The lower value of T_0 for the 0.2nm thick nitride layer indicates lower interaction energy and is related to the activation energy for hopping. The lower dependence on temperature for this thin layer indicates the likely higher contribution from non-temperature dependent direct tunneling between Si NCs. The increase of T_0 to a constant level and higher and more uniform dependence on $1/T^{1/2}$ for the thicker nitride layers indicate a transition to a regime dominated primarily by hopping over the barriers, rather than the tunneling through the thin barrier layers.

3. Discussion and conclusion

In this paper, We have successfully introduced UT-SiN barriers (0.2nm-2.0nm) into a Si-NC in SiC matrix material using a magnetron sputter system, for the purpose of isolate the SRC layer thus further prevent the inter-diffusion of SiC and subsequently eliminate the SiC crystallization in the matrix system.

From the structural characterization discussion, when Si_3N_4 layer thickness increase over 0.8nm, crystallization of the SiC matrix has been greatly suppressed and a clear layered super lattice structure can be observed in TEM image. This point have been well supported by the XRR investigation where clear Bragg peaks and Kiessing fringes still evenly distributed after very high temperature annealing. Meanwhile, Si NC grain size can also be well confined in this superlattice hybrid structure which is quantitatively proved in XRD measurement. The bonding energy of Si atom and C atom have been obtained by the XPS measurement, where the peak shift of the Si^{n+} is ascribed to the grain size change of Si NCs and the peak shift between C I and II position can be explained as the absence of SiC NC in the matrix.

The carrier hopping effect is likely to be the dominate carrier transport mechanism when the Si_3N_4 barrier thickness is greater than 0.8nm. Finally, we conclude that in future, a 0.5-0.8nm thick layer of Si_3N_4 barrier layer would be optimum to achieve both good Si-NC confinement and minimal film resistivity for a candidate material for photovoltaic applications.

In conclusion, the new hybrid super-lattice structure behaves superior characters than SRC / SiC super-lattice structure, from the points of layer isolation, Si NCs grain size confinement and SiC NC elimination. Significant band gap shift and relative high conductivity intrinsically (compare with silicon dioxide matrix [15]) of this material offers us a potential material candidate in “all-Si” tandem photovoltaic application.

References

1. Conibeer G, Green M, Cho E-C, König D, Cho Y-H, Fangsuwannarak T, Scardera G, Pink E, Huang Y, Puzzer T *et al*: **Silicon quantum dot nanostructures for tandem photovoltaic cells**. *Thin Solid Films* 2008, **516**(20):6748-6756.
2. Song D, Cho E-C, Conibeer G, Flynn C, Huang Y, Green MA: **Structural, electrical and photovoltaic characterization of Si nanocrystals embedded SiC matrix and Si nanocrystals/c-Si heterojunction devices**. *Solar Energy Materials and Solar Cells* 2008, **92**(4):474-481.
3. Cheng Q, et al.: **Structural evolution of nanocrystalline silicon thin films synthesized in high-density, low-temperature reactive plasmas**. *Nanotechnology* 2009, **20**(21):215606.
4. Kurokawa Y, Yamada S, Miyajima S, Yamada A, Konagai M: **Effects of oxygen addition on electrical properties of silicon quantum dots/amorphous silicon carbide superlattice**. *Current Applied Physics*, **In Press, Corrected Proof**.
5. Song D, Cho E-C, Conibeer G, Huang Y, Flynn C, Green M: **Structural characterization of annealed Si1-x Cx /SiC multilayers targeting formation of Si nanocrystals in a SiC matrix**. *Journal of Applied Physics* 2008, **103**(8):83544.
6. Benton JL, Kimerling LC, Stavola M: **The oxygen related donor effect in silicon**. *Physica B+C* 1983, **116**(1-3):271-275.
7. Molinari M, et al.: **Effects of the amorphous-crystalline transition on the luminescence of quantum confined silicon nanoclusters**. *EPL (Europhysics Letters)* 2004, **66**(5):674.
8. Comedi D, Zalloum OHY, Irving EA, Wojcik J, Roschuk T, Flynn MJ, Mascher P: **X-ray-diffraction study of crystalline Si nanocluster formation in annealed silicon-rich silicon oxides**. *Journal of Applied Physics* 2006, **99**(2):023518.
9. Isenberg J, Reber S, Warta W: **Diffusion Properties of Ion-Implanted Vanadium in PECVD-SiO[sub 2] and PECVD-SiN[sub x]**. *Journal of The Electrochemical Society* 2003, **150**(7):G365-G370.
10. Riabinina D, Durand C, Margot J, Chaker M, Botton GA, Rosei F: **Nucleation and growth of Si nanocrystals in an amorphous Si O2 matrix**. *Physical Review B* 2006, **74**(7):075334.
11. Kim S, Kim MC, Choi S-H, Kim KJ, Hwang HN, Hwang CC: **Size dependence of Si 2p core-level shift at Si nanocrystal/SiO[sub 2] interfaces**. *Applied Physics Letters* 2007, **91**(10):103113.
12. Lee RC, Aita CR, Tran NC: **The air-exposed surface of sputter deposited silicon carbide studied by x-ray photoelectron spectroscopy**. *Journal of Vacuum Science & Technology A: Vacuum, Surfaces, and Films* 1991, **9**(3):1351-1354.
13. Mulloni V, Bellutti P, Vanzetti L: **XPS and SIMS investigation on the role of nitrogen in Si nanocrystals formation**. *Surface Science* 2005, **585**(3):137-143.
14. Liu Y: **A study on Si nanocrystal formation in Si-implanted SiO2 films by x-ray photoelectron spectroscopy** *J Phys D: Appl Phys* 2003, **36**:L97.
15. Hao XJ, Cho EC, Flynn C, Shen YS, Park SC, Conibeer G, Green MA: **Synthesis and characterization of boron-doped Si quantum dots for all-Si quantum dot tandem solar cells**. *Solar Energy Materials and Solar Cells* 2009, **93**(2):273-279.
16. Balberg I, Savir E, Jedrzejewski J, Nassiopoulou AG, Gardelis S: **Fundamental transport processes in ensembles of silicon quantum dots**. *Physical Review B* 2007, **75**(23):235329.
17. Yakimov AI, Dvurechenskii AV, Nenashev AV, Nikiforov AI: **Evidence for two-dimensional correlated hopping in arrays of Ge/Si quantum dots**. *Physical Review B* 2003, **68**(20):205310.